Title

Beta2* Nicotinic Receptors Regulate Cognition and Social Behavior Through Functionally Distinct Neuronal Populations

Running title: Beta2* nAChRs in the PFC

Authors

Alice Abbondanza[1, 2], Jan Elias[3], Chandani R. Verma[1], Amanda Rosanna Alves Barboza[1], Martin Capek[4, 5], Trisha Jigar Dhabalia[1], Andrea Grigelova[6], Sylvie Dumas[7], Veronique Bernard[2], Helena Janickova[1]

Affiliations

[1], Laboratory of Cholinergic Signaling, Institute of Physiology of the Czech Academy of Sciences, Prague, 14200, Czech Republic

[2], Neuroscience at Sorbonne Université (NeuroSU), Institut de Biologie Paris Seine, Institut National de la Santé et de la Recherche Médicale, Centre National de la Recherche Scientifique, Sorbonne Université, Paris, 75005, France

[3], Institute of Molecular Genetics of the Czech Academy of Sciences, Czech Centre for Phenogenomics, Vestec, Czech Republic

[4], Laboratory of Advanced Microscopy and Data Analysis, Institute of Physiology of the Czech Academy of Sciences, Prague, 14200, Czech Republic

[5], Light Microscopy, Institute of Molecular Genetics of the Czech Academy of Sciences, Prague, 14200, Czech Republic

[6], Laboratory of Developmental Epileptology, Institute of Physiology of the Czech Academy of Sciences, Prague, 14200, Czech Republic

[7], Oramacell, Paris, 75006, France

Corresponding author: Helena Janickova, helena.janickova@fgu.cas.cz

Keywords: nicotinic acetylcholine receptors, prefrontal cortex, mice, behavior, FISH, CRISPR

Abstract

Beta2 subunit-containing nicotinic acetylcholine receptors (beta2* nAChRs) are highly expressed in the prefrontal cortex (PFC) and critically regulate behavioral and cognitive domains disrupted in neuropsychiatric disorders. Despite their therapeutic potential, the cell-type- and circuit-specific functions of beta2* nAChRs remain poorly defined, partially due to the lack of selective pharmacological tools. Here, we delineate the cellular expression patterns and behavioral roles of beta2* nAChRs across distinct neuronal populations of the mouse PFC. Using fluorescence in situ hybridization (FISH), we mapped beta2 nicotinic subunit expression across cortical layers and major neuronal classes. We then employed CRISPR-mediated knockdown (KD) to selectively reduce beta2* nAChRs expression in two distinct PFC neuronal populations and, for comparison, in a striatal population. Selective KD of beta2* nAChRs in deep-layer PFC neurons defined by early expression of neuropeptide Y (NPY) disrupted working memory and exploratory behavior and reshaped social and anxiety-like behaviors. In contrast, KD in superficial-layer PFC interneurons expressing the serotonin receptor 5HT3a induced a robust hypersocial phenotype, accompanied by exploratory behavior changes overlapping with those observed following NPY KD. Notably, KD of beta2* nAChRs in a rare NPY-expressing striatal population affected similar behavioral domains, but largely in the opposite direction to PFC manipulations. Together, these findings reveal opposing, cell-type- and region-specific contributions of beta2* nAChRs to behavioral regulations, highlighting the necessity of circuit-resolved targeting strategies to improve the precision and efficacy of therapeutic intervention for neuropsychiatric disorders.

Introduction

Neuronal nicotinic acetylcholine receptors (nAChRs) are pentameric ligand-gated ion channels composed of 12 subunits (α2-10, β2-4). Among them, heteromeric alpha4beta2* receptors (the asterisk indicating that additional subunits may be part of the pentamer) [1,2] represent one of the most abundant nicotinic receptor subtypes in the mammalian brain. They regulate fundamental neuronal processes, including neurotransmitter release, neuronal excitability and synaptic plasticity [3,4]. Their wide expression and essential physiological roles make them attractive therapeutic targets across a range of neuropsychiatric disorders [5].

The rodent prefrontal cortex (PFC) contributes to the higher-order cognitive and behavioral functions, including attention, memory, social interactions, and anxiety- and depression-like behaviors. These functions emerge from complex signaling within heterogeneous neuronal populations that differ in morphology, gene expression, electrophysiological properties, and circuit connectivity [6–8]. Alterations in PFC activity are commonly observed in neuropsychiatric disorders, including schizophrenia, autism spectrum disorder (ASD), anxiety, and depression [9–11]. Notably, many of these disorders have been linked to dysregulated nicotinic signaling and altered smoking behavior. For example, individuals with schizophrenia exhibit a markedly increased prevalence of heavy smoking, whereas individuals with ASD are less likely to smoke [12–14].

Many PFC neuronal populations express beta2 subunit-containing nAChRs (beta2* nAChRs) [8], and the contribution of prefrontal beta2* nAChRs to cognitive and behavioral regulation is well established [15,16]. Knockdown (KD) of beta2* nAChRs in the PFC induces a hypersocial phenotype, which can be reversed by re-expression of *Chrnb2*, the gene coding the beta2 subunit [17]. Prefrontal nAChRs have also been implicated in multiple behavioral and cognitive domains dependent on PFC function, including attention, working memory and cognitive flexibility [18–21].

Despite extensive investigation of beta2* nAChRs in the PFC, a detailed understanding of their expression and function across individual neuronal populations remains incomplete [6,18,22]. Functional beta2* nAChRs have been proposed to be present in layer VI pyramidal neurons, whereas in the other layers, they are thought to be expressed primarily in somatostatin-positive and some additional interneuron types [6]. In contrast, parvalbumin-positive interneurons are generally considered to lack functional beta2* nAChRs [6,9,18,23]. Much of this knowledge derives from electrophysiological studies that, while highly informative, do not provide population-level

quantification. Transcriptomic approaches can address this limitation, although information on laminar distribution is often lacking [7].

While expression studies and electrophysiological recordings have provided important insight into the cell-type-specific expression of beta2* nAChRs in the PFC, our understanding of their functional roles within defined neuronal populations remains even more limited. Most genetic and pharmacological manipulations to date have targeted the PFC globally or at the level of broad anatomical subregions [17,18,24], restricting insight into the cell-type-specific contributions of beta2* nAChRs to behavior [9]. This limitation has become increasingly salient as modern molecular approaches reveal extensive neuronal diversity, raising the possibility that perturbing the same receptor subtype in distinct neuronal classes may produce divergent circuit and behavioral outcomes. Importantly, the few studies that have examined nAChR function in a cell-ad circuit-specific manner suggest that receptors expressed by selective and relatively rare neuronal populations can exert disproportionately strong effects on behavior [9,25,26]. Therefore, a deeper understanding of the neuronal-type-specific role of beta2* nAChRs is essential for the development of more effective and safer therapeutic strategies targeting behavioral symptoms of neuropsychiatric disorders.

In this study, we address this gap by elucidating the expression patterns and functional significance of beta2* nAChRs in defined neuronal populations of the mouse PFC. We first performed a systematic analysis of beta2 subunit expression across cortical layers and individual neuronal types in the PFC. We then focused on two neuronal populations that differ markedly in abundance, laminar distribution and functional properties [27,28]. Neurons expressing neuropeptide Y (NPY) and interneurons expressing the serotonin receptor 5HT3a. Our primary objectives were to determine whether selective KD of the beta2 subunit in these populations produces reproducible behavioral phenotypes and to assess whether the behavioral consequences differ between cell types. To assess region-specific effects, we also examined the consequences of beta2* nAChR KD in NPY-expressing neurons of the dorsal striatum. All KD models were subjected to comprehensive behavioral testing of PFC-dependent domains commonly disrupted in neuropsychiatric disorders, thereby probing the functional and therapeutic relevance of beta2* nAChRs expressed by specific neuronal populations.

Methods and Materials

Animals

All procedures followed the European Community Council directive for laboratory animal use (2010/63/EU) and were approved by the Ethics Committee for animal experimentation of the Czech Academy of Sciences. Only male mice were used due to resource limitations. Tissue for FISH, qPCR, T7 assay and radioligand binding was collected from 2-3-month-old mice. The following lines were used: C57BL/6 wild-type (WT) mice; beta2-flox/flox mice [29] carrying floxed exon 5 of *Chrnb2*; Rosa26-floxed STOP-Cas9 knock-in mice with Cre-inducible Cas9-2A-EGFP expression [30]; and two Cre-driver lines expressing Cre under the Npy or Htr3a promoters [31,32]. Details of all lines are provided in Supplementary Table S1.

Experimental design and statistical analysis

Mice were semi-randomly assigned so that each cage contained animals from both control and experimental groups. To assess reproducibility, selected behavioral experiments were performed in two independent cohorts originating from different housing facilities and tested more than 12 months apart. Behavioral outliers were defined as values exceeding the mean ± 2 SD and were removed from all parameters within that experiment. After behavioral testing, brains were examined for AAV expression; animals lacking expression were excluded. Statistical analyses were performed in GraphPad Prism (version 10). Two-tailed t-tests were used for comparison between two groups, and two-way ANOVA with Sidak's post-hoc test was used for analyses involving two variables. All graphs show mean ± SEM.

Double-probe fluorescence in situ hybridization (FISH)

FISH was performed as previously reported [33,34]. Brains were sectioned at 16 µm thickness. Digoxigenin (DIG)- or fluorescein-labelled RNA probes were synthesized using in vitro transcription with labelled nucleotides (Sigma-Aldrich; Reference 11277073910 and 11685619910). Sections were fixed in 4 % paraformaldehyde (PFA) and acetylated in 0.25 % acetic anhydride/100 mM triethanolamine. Hybridization was performed for 18 h at 65 °C in formamide buffer containing 1 µg/ml of each riboprobe. Sections were washed in decreasing-strength SSC buffers at 65 °C and blocked with 20 % fetal bovine serum (FBS) and 1 % blocking solution. DIG was detected with HRP-anti-DIG Fab fragments (1:2500; Sigma-Aldrich; Reference 11207733910) and visualized with Cy3-tyramide (1:100). Fluorescein was detected

with HRP-anti-fluorescein Fab fragments (1:5000; Sigma-Aldrich; Reference 11426346910) and revealed using Cy2-tyramide (1:250). Slides were scanned at 20x resolution using a NanoZoomer 2.0-HT system (Hamamatsu, Japan), and images were analyzed with NDP.view2 (Hamamatsu Photonics) and QuPath [35]. Regions of interest were defined using the Paxinos atlas [36].

Quantitative PCR (qPCR)

RNA was extracted using TriPure reagent (Roche), DNase-treated, and reverse-transcribed using LunaScript RT SuperMix (NEB). qPCR was performed using gb SG PCR Master mix (Generi Biotech).

AAV vectors and CRISPR/Cas9 gene editing

AAV-U6-sgRNA-hSyn-mCherry vectors expressed single guide RNA (sgRNA) (Addgene #87916). We used a previously validated [37] sgRNA targeting (sequence: ATCAGCTTGTTATAGCGGGA) and a scrambled control sgRNA (GCGAGGTATTCGGCTCCGCG). The sgRNA was expressed from the U6 promoter, and mCherry from the hSyn promoter. Cloning followed established protocols [38]. Vectors were packaged into the AAV5 (UNC Vector Core) at titers of 1 x 10 [12-13] vg/ml.

Stereotaxic surgeries

Mice were anesthetized with ketamine/xylazine (Vetoquinol, bioveta). PFC stereotaxic coordinates were AP +2.5/+2.2, ML±0.4/±0.3, DV -1.9/-2.1. Dorsal striatum (DS) coordinates were AP +1.4, ML ±1.6, DV -3.5/-2.6. Injections (500 nl each)were made using a microinjection pump (MICRO-2T-UMP3-NL2010, World Precision Instruments) at 50 nl/min. AAV expression was verified via mCherry fluorescence. Double-positive cells were counted in sections spaced by 0.2 mm apart from +2.8 to +1.6 relative to bregma.

Radioligand binding with [3H]epibatidine

Membranes were prepared from PFC tissue expressing AAV vectors. NPY-Cre::Cas9-GFP mice were injected with sgRNA-Chrnb2 or control sgRNA-scr; beta2-flox/flox mice received AAV5-CMV-Cre-GFP or AAV5-CMV-GFP. To maximize labeled tissue, three injections (500 nl each) were made across AP +2.8/+2.4/+2.0, ML 0, and DV -1.5/-2.0/-2.2. Three weeks later, tissue showing fluorescence was dissected, homogenized in PBS with protease inhibitors, and

centrifuged. Protein concentration was measured via Lowry's assay [39]. Membrane homogenates were incubated with 0.2 nM [3H]epibatidine (62.2 Ci/mmol, Perkin-Elmer) overnight at 4 °C. Samples were filtered through polyethyleneimine-soaked GFC filters, and radioactivity was measured with a scintillation counter (Tri-Carb, Perkin-Elmer).

T7 endonuclease assay

The assay followed the manufacturer's instructions (T7 Endonuclease Detection Assay Kit, Sigma-Aldrich). Tissue was collected from three sgRNA-Chrnb2-injected NPY-Cre::Cas9 mice, two sgRNA-scr controls, and one non-injected mouse. DNA was extracted by phenol-chloroform. The targeted Chrnb2 region was amplified using Phusion High-Fidelity polymerase (ThermoFisher), denatured, reannealed, and digested with T7 endonuclease to detect CRISPR-induced mismatches.

Behavioral testing

The behavioral tests were performed in the following order: the open field (OF) test, social preference test, social memory test (omitted in Htr3a-Cre::Cas9-GFP mice), hole-board test, Y-maze spontaneous alternations test, novel object recognition (NOR) test, light/dark test, tail suspension test (TST), elevated plus maze (EPM), social interaction (SI) and the forced swim test (FST). All tests except the light/dark test were conducted during the light phase of the light/dark cycle, in a dedicated testing room. The details on the individual test can be found in the Supplementary material.

Results

Analysis of beta2* nAChRs expression in specific neuronal types in the mouse PFC

We first used FISH to analyze *Chrnb2* expression in major PFC neuronal populations (Fig. 1A). Across bregma levels (+2.8-+1.6), *Chrnb2* expression was stable (Suppl. Fig. S1A). Layer analysis showed fewer *Chrnb2+* cells in layer I than in all other layers, with no major differences elsewhere (Suppl. Fig. S1B). We then examined *Chrnb2* expression in excitatory *Vglut1+* neurons and in five inhibitory populations: neuropeptide Y-positive (*Npy+*), vasoactive intestinal peptide-positive (*Vip+*), serotonin receptor 5HT3a-positive (*Htr3a+*), parvalbumin-positive (*Pv+*) and somatostatin-positive (*Sst+*) neurons (Fig. 1B-C). Their distribution was layer-dependent and matched published data [40,41]; *Vip+* and *Htr3a+* neurons were enriched in the superficial layers, whereas the others predominated in deeper layers (Fig. 1E-F).

Then we examined the proportion of *Chrnb2+* cells in each population. Surprisingly, layer had little effect on the percentage of *Chrnb2+* cells within each population, except for *Vip+* neurons, which showed increased expression in layer VI (Suppl. Fig. S1C). Therefore, we averaged the data across layers (Fig. 1G). All neuronal types expressed *Chrnb2*, with the highest levels in *Pv+* neurons (nearly all *Pv+* cells), followed by *Vglut1+* neurons (~80 %). *Npy+* and *Htr3a+* populations showed similar expression (~70 %), while *Vip+* neurons expressed *Chrnb2* least (~50 %) (Fig. 1G). We also quantified the contribution of each population to total *Chrnb2* expression (Fig. 1H). It was mostly dependent on their overall layer distribution, with the notable exception of *Vip+* neurons in layer VI (see above), which increased their contribution due to the higher *Chrnb2* expression in that layer (Fig. 1H, Suppl. Fig. S1C). In addition, in layer VI, nearly all *Chrnb2+* cells belonged to the examined types, whereas in superficial layers, *Chrnb2+* cells exceeded their combined contribution. It suggests additional unprofiled cell types contributing to *Chrnb2* expression in the upper layers. Overall, *Chrnb2* mRNA was detected in most PFC neurons, with population identity more influential than layer localization.

CRISPR KD of the beta2 nicotinic subunit in NPY-expressing neurons

Given the widespread expression of beta2* nAChRs, we next tested whether selective KD in a single neuronal population would yield a reproducible behavioral phenotype and whether the phenotype would diverge between different targeted populations. To test this, we chose two neuronal populations that exhibited significant differences in their number, laminar distribution

and presumed functional role within the local circuits, NPY- and 5HT3A-expressing neurons (Fig. 1D, G, H). In contrast to 5HT3A-expressing neurons, the NPY-expressing neurons showed a substantial contribution to *Chrnb2* expression across layers, with a clear enrichment in deeper layers (Fig. 1H). They were also previously shown to control the PFC-dependent anxiety-like behavior through a direct inhibition of projection pyramidal neurons [42]. To achieve neuron- and region-specific KD via CRISPR, we crossed NPY-Cre mice with a Cre-dependent Cas9-GFP line [30,31]. In the NPY-Cre::Cas9-GFP mice, GFP expression largely matched adult NPY patterns in subcortical regions. However, in the cortex, it was more abundant, particularly in deep layers (Fig. 2A, B), consistent with transient developmental NPY promoter activity [43]. In support of this hypothesis, FISH confirmed strong overlap between *Cre* and *Npy* mRNA (Fig. 2C, D) and minimal overlap between *Gfp* and *Npy* (Fig. 2E, F).

FISH-based cell-type analysis showed that ~70 % of GFP+ cells were excitatory (*Vglut1*+) and 30 % inhibitory (*Viaat*+). The inhibitory neurons were mostly represented by *Sst*+ neurons (16 %) and *Pv*+ neurons (13 %), which is in line with previous reports [27]. To a lesser extent, we identified *Htr3a*+ neurons (2.1 %) and *Vip*+ neurons (1.4 %) (Fig. 2G-J). Thus, subsequent experiments targeted beta2* nAChRs in neurons with early expression of NPY (here labelled as eeNPY neurons), located mainly in deep layers and spanning both excitatory and inhibitory neuronal types.

To induce KD, NPY-Cre::Cas9-GFP mice were injected with AAV-sgRNA-*Chrnb2* (Fig. 3A-C), yielding expression across +2.8-+1.6 mm from bregma (Fig. 3A-C). Some mice showed unilateral expression but were retained in the study. The number of double-positive (GFP+mCherry+) cells did not differ between sgRNA-scr and sgRNA-Chrnb2 groups (Fig. 3D). To confirm the efficiency of our KD approach, we first measured the binding of beta2* nAChRs radioligand [3H]epibatidine in brain homogenates obtained from NPY-Cre::Cas9-GFP mice injected with sgRNA-Chrnb2 and sgRNA-scr. However, we could not detect any difference in the [3H]epibatidine binding between the control and sgRNA-Chrnb2 injected mice or even in beta2-fx/fx mice crossed with the NPY-Cre line, likely due to the low proportion of double-positive neurons in the homogenate (Fig. 3E). The [3H]epibatidine binding showed only a modest decrease in homogenates from beta2-flox/flox mice injected with AAV5-CMV-Cre vector, inducing beta2* nAChRs deletion in all transduced cells (Fig. 3E, right). This points to the fact that even after the complete deletion, the beta2* nAChRs expressed on terminals

projecting from other brain regions remained intact. Given the absence of reliable beta2-targeting antibodies, we used the T7 endonuclease assay to confirm that CRISPR indels were present only in sgRNA-Chrnb2-injected homogenates (Fig. 3F).

KD of beta2* nAChRs in the eeNPY-Cre neurons leads to working memory impairment and changes in exploratory behavior

To test whether the selective KD leads to reproducible changes in behavior, we tested our control and mutant mice in a battery of behavioral tasks (Fig. 4A), probing potential changes in motor activity, exploratory behavior, working memory, social and anxiety-like behavior, and passive coping behavior (Fig. 4C- H, Suppl. Fig. S2, Suppl. Fig. S3A-C). Two independent cohorts were analyzed to ensure reproducibility, and we present merged data for both cohorts as well as separate data for each individual cohort (green, blue, and red graphs in Fig. 4 and Suppl. Fig. S2, S3). During the initial characterization of the NPY-Cre model, we also found a potential effect of the NPY-IRES-Cre allele on the NPY expression (Fig. 4B). To avoid any confounding effects of altered NPY expression, only NPY-Cre heterozygotes were used in all behavioral experiments.

The selective beta2* nAChRs KD in PFC eeNPY-Cre neurons impaired working memory, as evidenced by reduced alternations in the Y-maze (Fig. 4C). This effect was observed in both cohorts, although in cohort 2 did not reach significance, likely due to the lower sample size. The overall locomotor activity in the Y-maze was not affected (Fig. S2F). In the NOR test, mutants displayed more interactions with the objects, particularly the novel object, across both cohorts (Fig. 4D). Interestingly, the total interaction time was less affected (Fig. S2H), which indicates mutants' tendency to explore the novel object repeatedly, resulting in a higher number of shorter interactions, suggesting repeated novelty checking rather than sustained exploration. In addition to impairment of working memory and exploration, changes in social behavior emerged, but they were less consistent across cohorts: a modest decrease in social preference became significant only when data from both cohorts were pooled (Fig. 4E), and a similar effect, an increased interest in the object stimulus compared to mouse, was found only in cohort 2 in the social interaction test (Fig. 4G). In contrast, an increased interest in the novel social stimulus during the social memory test was observed only in cohort 1 (Fig. 4F). Finally, a strong anxiolytic phenotype in the EPM was observed in cohort 1 but not in cohort 2 (Fig. 4H). Other behavioral tests showed no effect of the beta2* nAChRs KD in the targeted population, including locomotor

activity (open field test), repetitive behavior (hole-board test), anxiety-like behavior (light-dark box test), and passive coping behavior (TST and FST tests) (Fig. S2).

All tested behavioral parameters were used in principal component analysis (PCA), and grouped based on their contributions to individual principal components. When transformed to PC scores, we found a significant difference in PC1 between control and mutant mice only for cohort 1 (Fig. S3D). In this cohort, the PC1 was primarily driven by variables derived from the EPM task, and thus, the difference was not reproduced in cohort 2. We also checked whether the differences between cohorts can be related to differences in the AAV transduction efficiency. We found that cohort 2 showed a significantly higher number of double-positive cells in the PFC, primarily in control animals (Fig. S3E). When we correlated selected behavioral parameters with the number of double-positive cells in control and mutant animals in both cohorts (Fig. S3F-H), we found a significant but indirect correlation between the number of double-positive cells and the number of interactions with a novel object in the NOR test in mutant mice (Fig. S3G).

Due to the inconsistent findings in the EPM test across cohorts, we prepared a new cohort that was tested in selected tests both before and after the AAV-sgRNA injection (Fig. S4). Supporting our previous findings, the AAV-sgRNA injection increased the preference for the object and for the novel mouse in the social preference and memory task (Fig. S4G-H). Importantly, baseline anxiety assessed by EPM was lower in future mutants randomly pre-assigned before the surgery, but it reversed afterward, and only mutants showed significant pre- vs. post-injection shifts (Fig. S4B-D). These data indicate that beta2* nAChRs KD affects anxiety-like behavior, but the effect is complex and dependent on other variables, such as prior exposure to the environment. Overall, KD in eeNPY-Cre neurons produced reproducible impairments in working memory and altered exploratory behavior, while effects on social and anxiety-like behavior were more subtle and sensitive to environmental, cohort-specific factors.

KD of beta2* nAChRs in the 5HT3A-expressing PFC neurons leads to partially overlapping but distinct behavioral changes

To test whether beta2* nAChRs in another PFC population contribute differently to behavior, we targeted 5HT3A+ interneurons. As we showed previously (Fig. 1, Fig. S1), *Chrnb2* expression in 5HT3A+ neurons is comparable to NPY+ neurons, but they are sparser and preferentially distributed in the upper layers [28], suggesting involvement in gating a local disinhibitory circuit

[44,45]. We crossed the Htr3a-Cre mice [32] with the Cas9-GFP line (Fig. 5A). The Cre-GFP expression in Htr3a-Cre::Cas9-GFP mice in the PFC was very different from the expression observed in NPY-Cre::Cas9-GFP. Consistent with our FISH data (Fig. 1E), Cre-GFP-positive neurons were relatively sparse and, although present in all cortical layers, were enriched in the upper layers (Fig. 5A). Htr3a-Cre::Cas9-GFP mice received AAV-sgRNA injections, and the AAV-sgRNA (mCherry) expression was examined in all mice used for behavior. The double-positive cell counts were similar between groups (Fig. 5B, C).

Beta2* nAChRs KD in 5HT3A+ neurons produced behavioral changes that were partially similar to those observed in NPY-Cre::Cas9-GFP mice but also showed some major differences (Fig. 5D-H, Fig. S5). Most importantly, in contrast to eeNPY+ neurons, the beta2* nAChRs KD in 5HT3A+ neurons led to a pronounced hypersocial phenotype. In the social preference test, mutant mice spent more time interacting with the social stimulus compared to controls (Fig. 5G). When expressed in relative values, the 5HT3A+ mutant mice showed a higher preference for the social vs. non-social stimulus compared to controls, which is opposite to the findings in eeNPY+ mutants (Fig. 4E, Fig. 5G). In the social interaction test, where the social and non-social stimuli are not presented at the same time, Htr3a-Cre::Cas9-GFP mutant mice showed changes mirroring those found in NPY-Cre::Cas9-GFP mutants (Fig. 4G, 5F).

In addition, the beta2* nAChRs KD in the two neuronal populations resulted in similar impairments of working memory and exploratory behavior. However, a trend to a decreased alternation score in the Y-maze did not reach significance in 5HT3A+ mutants (Fig. D), possibly because the disrupting effect was weaker given the relative scarcity of 5HT3A+ neurons. The NOR phenotype previously found in eeNPY+ mutants was largely reproduced in 5HT3A+ mutants. The mice showed more interactions with both old and new stimuli (Fig. 5E), while the total interaction time was not increased (Fig. S5E), indicating more repeated and shorter interactions rather than sustained exploration. Lastly, anxiety-like behavior remained unchanged (Fig. 5H), and no additional behavioral phenotypes were detected in 5HT3A+ mutants.

KD of beta2* nAChRs in the NPY-expressing striatal interneurons leads to changes opposite to those in the PFC KD

Finally, we wanted to compare behavioral differences associated with targeting distinct neuronal populations, with the effect of inter-regional differences. To do that, we used our CRISPR

approach to induce beta2* nAChRs KD in NPY-expressing interneurons in the dorsal striatum. In contrast to abundant cortical expression, striatal Cas9-GFP expression was sparse and consistent with adult NPY patterns (Fig. 6A). We previously showed that only ~6 % of striatal NPY interneurons express *Chrnb2* [33], and thus we expected a relatively weak effect of the beta2* nAChRs KD on behavior. NPY-Cre::Cas9-GFP mice injected in the dorsal striatum underwent the same behavioral tests as the previous PFC cohorts (Fig. 6B, Fig. S6).

The beta2* nAChRs KD affected behavioral domains similar to those observed in the PFC cohorts, including changes of explorative behavior in the NOR test, sociability in the social preference test and anxiety-like behavior in EPM (Fig. 6 C-F). However, interestingly, changes observed after the KD in the dorsal striatum were mostly opposite to those observed after PFC KD. Mice with striatal KD exhibited a lower number of object interactions in the NOR test (Fig. 6C), with no effect on total exploration time (Fig. S6I, J). Furthermore, they exhibited an increased sociability in the social preference test (Fig. 6D) and an anxiolytic-like phenotype in the EPM (Fig. 6E). Working memory was not affected (Fig.S6G), and no additional phenotype was observed in this group.

Discussion

In this study, we examined the expression and behavioral significance of beta2* nAChRs across several neuronal populations in the PFC and dorsal striatum. We demonstrate that beta2* nAChRs are robustly expressed in all major neuronal types in the PFC and that selective KD of these receptors produces partially overlapping yet distinct - and in some cases opposing - behavioral effects. Although the specific behavioral manifestations varied between neuronal populations, the functional domains affected by beta2* nAChRs KD were remarkably consistent across neuronal types and brain regions. In the PFC, KD of beta2* nAChRs in the eeNPY population altered working memory, exploratory behavior, social behavior and, with greater variability, anxiety-like behavior. In contrast, targeting the KD to 5HT3A+ interneurons - a population that differs substantially in abundance and laminar distribution - resulted in a prominent hypersocial phenotype, clearly distinguishing the behavioral outcomes of KD in these two neuronal populations. Finally, KD of beta2* nAChRs in NPY+ interneurons of the dorsal striatum affected similar behavioral domains, with the notable exception of working memory, consistent with the established role of the PFC, but not the dorsal striatum, in this cognitive function [46]. Across all KD groups, we observed no changes in motor activity, passive coping behavior, or compulsive/stereotypic behavior.

Our FISH analysis demonstrated that beta2* nAChRs are expressed across all major neuronal types in the PFC, partly contrasting with conclusions from previous electrophysiological studies [6,22,47]. Although mRNA detection does not guarantee the presence of functional receptors, our work provides a systematic analysis of *Chrnb2* expression by the main PFC populations, revealing that a substantial proportion of these neurons expresses detectable levels of beta2 subunit mRNA. Importantly, the expression of *Chrnb2* within a given neuronal type was largely unaffected by bregma level or cortical layer, remaining relatively stable across the rostrocaudal axis and cortical depth (Fig. S1). *Vip*+ neurons in layer VI were a notable exception, showing markedly higher *Chrnb2* expression compared to more superficial layers. This may indicate the existence of subpopulations within the *Vip*+ class as previously proposed [41]. We also observed substantial variability in *Chrnb2* expression within the *Sst*+ population across sections (Fig. 1G), but this variability did not correlate with bregma position or other identifiable parameters.

While Chrnb2 expression remained stable within neuronal types across layers, the relative abundance of most neuronal types increased in deeper layers (Fig. 1D, E). Accordingly, in layer VI the examined neuronal types accounted for nearly all Chrnb2+ cells, whereas in superficial layers a considerable proportion of Chrnb2+ cells could not be assigned to the profiled populations (Fig. 1H). Technical factors, such as differences in probe sensitivity or limitations in image analysis, may partially contribute to this discrepancy. However, the proportion of unidentified Chrnb2+ cells suggests that additional, uncharacterized cell types may contribute to beta2* nAChRs expression in upper layers. Additionally, Layer I of the PFC is largely devoid of neuronal somata and is dominated by dendritic and axonal processes, including long-range cortical and subcortical projections. Therefore, it is likely that the puncta of the FISH signal in Layer I are largely not nuclear [48].

One unexpected observation in this study was the high prevalence of eeNPY neurons in deep cortical layers in the NPY-Cre::Cas9-GFP model. This aberrant cortical expression was not reported in the original characterization of this line 31, but similar findings have been noted elsewhere 43. We propose that this pattern reflects early developmental NPY promoter activity in neural progenitor cells that later give rise predominantly to deep-layer cortical neurons with prominent output connectivity. Whether and to what extent these eeNPY neurons constitute a functionally distinct population remains to be determined.

A central question of this study was whether selective targeting of nAChRs could enable more efficient, precise, and predictable modulation of behavioral and cognitive phenotypes. Our findings indicate that receptor manipulations restricted to specific neuronal populations or brain regions can indeed yield divergent behavioral outcomes, including hyper- versus hypo-social phenotypes and opposing effects on exploratory and anxiety-like behaviors. Notably, KD of beta2* nAChRs in the 5HT3A+ population produced a robust hypersocial phenotype, whereas KD in eeNPY neurons resulted in a comparatively weaker hyposocial effect (Fig. 4E, 5G). This difference may relate to the cellular composition of these populations, as 5HT3A+ neurons constitute a relatively homogeneous inhibitory population, whereas eeNPY neurons comprise a mixed population of excitatory and inhibitory cells (Fig. 2). Consistent with this interpretation, previous studies have shown that deletion of beta2* nAChRs in the PFC induces a hypersocial phenotype [17], potentially mediated by altered GABAergic interneuron function, as PFC inhibitory interneurons were previously linked to a hypersocial phenotype [49–51]. In addition, we

observed an increased preference for a social stimulus following KD of beta2* nAChRs in NPY+ striatal interneurons (Fig. 6D). This finding supplements our earlier work demonstrating that a broad, non-selective KD of beta2* nAChRs in striatal neurons leads to reduced sociability in mice [33]. Our findings suggest that therapeutic strategies targeting beta2* nAChRs may require neuronal-type-specificity to effectively correct social deficits.

All behavioral domains affected by our receptor manipulations have previously been linked to nicotinic signaling [17,33,52–57]. Despite the differences in directionality, the broader behavioral domains affected by the different KDs remained strikingly consistent. These recurrent alterations may reflect the pharmacological properties of beta2* nAChRs, including their affinity for acetylcholine (ACh). These properties may render them particularly responsive to ACh fluctuations under specific task conditions, such as novelty and arousal state. Future studies should directly test how beta2* nAChRs-mediated behavioral control is modulated by altered ACh levels, for example, by using acetylcholinesterase inhibitors. In addition, monitoring ACh dynamics during behavioral tasks, as performed in previous work [58], would also be highly informative. Because ACh levels vary with vigilance and arousal [59], fluctuations in these states may help explain why some anxiety and social measures differed across cohorts. Differences in baseline stress associated with distinct housing facilities, or subtle variations in the characteristics of social stimuli, may also have contributed. Moreover, because NPY release is itself stress-sensitive [60,61], nicotinic modulation of eeNPY neurons may exert distinct effects under different baseline stress conditions.

In conclusion, we demonstrated that even widely expressed neurotransmitter receptor subtypes, such as beta2* nAChRs, can exert distinct functional roles depending on the neuronal population in which they are expressed. Moreover, even a sparse population of receptors can shape behavior, as indicated by the effects of beta2* nAChRs KD in striatal NPY interneurons, a population with low *Chrnb2* expression [33]. This neuronal-type specificity should be taken into account when investigating receptor function and when designing targeted interventions to modulate behavioral symptoms. Emerging technologies that integrate pharmacological and genetic approaches [62–64] can enable us to exploit the complexity of receptor expression and function in a neuronal-type-specific manner. Ultimately, such precision may open new avenues for selective, effective targeting of neurotransmitter receptors in clinical practice.

Acknowledgements

We thank Dr. Cecilia Gotti for her help with the [3H]epibatidine binding experiments. We thank Dana Ungerova for her technical assistance. This work was supported by the Czech Ministry of Education, Youth and Sport (MSMT), project ERC CZ LL2402. We acknowledge the Light Microscopy Core Facility, IMG, Prague, Czech Republic, supported by MEYS – LM2023050, MEYS – CZ.02.1.01/0.0/0.0/18_046/0016045 and MEYS – CZ.02.01.01/00/23_015/0008205, for their support with the imaging and image analysis presented herein. Supported also by IPHYS BIF – MEYS CR (Large RI Project LM2023050 Czech-BioImaging) and ERDF (Project No. CZ.02.1.01/0.0/0.0/18_046/0016045). We thank Marie-Laure Niepon of the Image Platform at the Institute of Vision in Paris, France, for scanning the FISH slides.

Author Contributions

A.A., S.D., V.B. and H.J. designed research. A.A., J.E., C.R.V., A.R.A.B., T.J.D., S.D. and H.J. performed research. A.A., C.R.V., A.R.A.B., M.C., A.G., S.D. and H.J. analyzed data. H.J. and C.R.V. wrote the paper. A.A. and V.B. edited the paper.

Conflict of Interests

Nothing to declare.

Data Availability

The data generated and analyzed in this study are available from the corresponding author upon request.

Figure legends

Figure 1

Expression of beta2* nAChRs by different neuronal populations of the mouse PFC. (A) Anatomical areas examined by the FISH analysis are highlighted in grey. (B) Examples of sections stained for *Npy/Chrnb2* colocalization, showing DAPI (blue), *Npy* (green), and *Chrnb2* (magenta). (C) Overlay images of *Chrnb2* probe (magenta) colocalized with probes for markers of individual neuronal populations (green): *Vip*, *Htr3a*, *Pv*, *Sst* and *Vglut1*. (blue: DAPI). (D) The percentage of cells positive for markers of the main inhibitory populations across PFC cortical layers. Layer vs. neuronal type interaction, $F_{(12, 179)}=2.96$, p=0.0009. Two-way ANOVA. (E) The percentage of cells positive for the excitatory marker *Vglut1* across PFC cortical layers. Main effect of layer: $F_{(3, 16)}=6.49$, **, p=0.0044. One-way ANOVA. (F) A scheme of four cortical layers in the medial PFC. (G) The percentage of cells expressing *Chrnb2* in the main PFC neuronal populations. Each symbol shows an average per section (averaged left and right hemisphere). Main effect of neuronal type, $F_{(5, 19)}=9.8$, p<0.0001. Welch's one-way ANOVA. *, p<0.05, **, p<0.01, ****, p<0.0001. Dunnett's multiple comparisons test. (H) The proportion of major PFC neuronal types out of all *Chrnb2*+ cells across PFC layers. PrL=prelimbic cortex, IL=infralimbic cortex.

Figure 2

Characterization of the NPY-Cre mouse line. (A, B) Brain sections from NPY-Cre::Cas9-GFP mice showing widespread Cas-GFP expression in the cortex, primarily in layers V-VI. (C, D) Example of FISH images and quantification of the *Cre* and *Npy* mRNA colocalization, documenting a specificity of the NPY-Cre::Cas9-GFP model in adult mice. (E, F) Example of FISH images and quantification of the *Gfp* and *Npy* mRNA show modest overlap, indicating a significant early Cre expression during development. (G) Example brain sections stained with FISH, showing Gfp (green) and Vglut1 or Viaat signal (red). (H) Proportion of excitatory and inhibitory neurons within the Cas9-GFP-expressing population. (I) Examples of FISH staining, showing Gfp (green) and the individual IN markers (left to right: Sst, Pv, Htr3a, Vip) (red). (J)

Proportion of individual types of inhibitory INs within the Cas9-GFP-expressing population. cc=corpus callosum.

Figure 3

Evaluation of the KD of the beta2 nicotinic subunit induced by CRISPR. (A) A scheme of the KD strategy. (B) Stereotaxic coordinates and other parameters of the AAV-sgRNA injections. (C) An example of the AAV-sgRNA-Chrnb2 injected area. Left image and bottom close-up: Colocalization of the AAV-sgRNA vector (red) and nuclear staining (blue). Right image and top close-up: Colocalization of the AAV-sgRNA vector (red) and Cas9-GFP (green) expression in the NPY-Cre mouse model. (D) Number of neurons double-positive for Cas9-GFP and AAV-sgRNA (mCherry) counted in sections from control (sgRNA-scr) and mutant (sgRNA-Chrnb2) NPY-Cre::Cas9-GFP mice that were used for behavioral analysis. Control vs. mutant mice, 95% CI for the difference between means [-88; 220], p=0.393, two-tailed t-test. (E) [3H]epibatidine binding in brain homogenates from NPY-Cre::Cas9-GFP mice injected with AAV-sgRNA-Chrnb2 (left), NPY-Cre::beta2-flox/flox mice (middle) and beta2-flox/flox mice injected with AAV-Cre (right). NPY-Cre::Cas9: ctrl vs. mutant mice, 95% CI for the difference between means [-192; 148], p=0.770. NPY-Cre::beta2-flox/flox: Cre- vs. Cre+ mice, 95% CI for the difference between means [-231; 100], p=0.379. Beta2-flox/flox: GFP- vs. Cre-GFP-injected mice, 95% CI for the difference between means [-151; -25], p=0.0132, all by two-tailed t-test. (F) Results of the T7 assay demonstrating CRISPR-induced mismatches in the *Chrnb2* gene. Means ±SEM are shown in all graphs. PFC=prefrontal cortex.

Figure 4

KD of beta2 nicotinic subunit in NPY-Cre-positive population leads to specific changes in behavior. (A) An overview and the order of behavioral tests performed in NPY-Cre::Cas-GFP mice injected with sgRNA-scr (controls) or sgRNA-Chrnb2 (mutants). Tests showing behavioral alterations in mutants are highlighted in blue color. (B) Expression of *Npy* mRNA in WT vs. NPY-Cre::Cas9-GFP mice. 95% CI for the difference between means [-77; 0.76], p=0.054, two-tailed t-test. (C-H) Results of tests showing behavioral alterations in NPY-Cre::Cas9-GFP mutant

animals. All tests were performed in two independent cohorts. Pooled data are shown on the left (green graphs, n(ctrl)=21-22, n(mutant)=24-27), cohort 1 in the middle (blue graphs, n(ctrl)=9-11, n(mutant)=12-13) and cohort 2 on the right (red graphs, n(ctrl)=11-13, n(mutant)=11-14). Means ±SEM are shown in all graphs. (C) Spontaneous alternations Y-maze test, alternation score in ctrl vs. mutant mice. Pooled cohorts: 95 % CI [-12.2; -3.9], p=0.0003. Cohort 1: 95 % CI [-13.2; -1.3], p=0.0199. Cohort 2: 95 % CI [-11.8; 1.0], p=0.096, all by two-tailed t-test. (D) Novel object recognition test, number of interactions in ctrl vs. mutant mice. Pooled cohorts, effect of genotype: $F_{(1, 88)}$=6.4, p=0.013; number of interactions with the new object in ctrl vs. mutant mice, p=0.036. Cohort 1, genotype x object interaction: $F_{(1, 38)}$=6.6, p=0.014; number of interactions with the new object in ctrl vs. mutant mice, p=0.015. Cohort 2, effect of genotype: $F_{(1, 44)}$=13, p=0.0007; number of interactions with the new object in ctrl vs. mutant mice, p=0.0258. Two-way ANOVA with Sidak's post hoc comparison test. (E) Social preference test, interaction time in ctrl vs. mutant mice, genotype x stimulus interaction. Pooled cohorts: $F_{(1, 94)}$=7.7, p=0.007. Cohort 1: $F_{(1, 44)}$=1.2, p=0.28. Cohort 2: $F_{(1, 50)}$=3.1, p=0.8. Two-way ANOVA. (F) Social memory test, interaction time in ctrl vs. mutant mice, genotype x stimulus interaction. Pooled cohorts: $F_{(1, 94)}$=2.4, p=0.1192. Cohort 1: $F_{(1, 42)}$=10, p=0.002. Cohort 2: $F_{(1, 50)}$=0.1, p=0.71. Two-way ANOVA. (G) Social interaction test, interaction time in ctrl vs. mutant mice, genotype x stimulus interaction. Pooled cohorts: $F_{(1, 88)}$=2.6, p=0.11. Cohort 1: $F_{(1, 38)}$=4, p=0.0506. Cohort 2: $F_{(1, 42)}$=12, p=0.0013. Two-way ANOVA. (H) Elevated plus maze, time in arms in ctrl vs. mutant mice, genotype x arm interaction. Pooled cohorts: $F_{(1, 86)}$=2.3, p=0.13. Cohort 1: $F_{(1, 40)}$=34, p<0.0001. Cohort 2: $F_{(1, 42)}$=0.5, p=0.45. Two-way ANOVA.

Figure 5

KD of beta2 nicotinic subunit in Htr3a-Cre-positive PFC neurons increases sociability. (A) A representative brain section from Htr3a-Cre::Cas9-GFP mouse showing scattered Cas-GFP expression in the cortex, predominantly in superficial layers. (B) An overview and the order of behavioral tests performed in Htr3a-Cre::Cas-GFP mice injected with sgRNA-scr (controls) or sgRNA-Chrnb2 (mutants). Tests showing behavioral alterations in mutants are highlighted in blue. (C) Number of neurons double-positive for Cas9-GFP and AAV-sgRNA (mCherry) counted in sections from control (sgRNA-scr) and mutant (sgRNA-Chrnb2) Htr3a-Cre::Cas9-

GFP mice that were used for behavioral analysis (only in cohort 1). n(ctrl)=9, n(mutant)=11. 95% CI for the difference between means [-59; 85], p=0.71, two-tailed t-test. (D-H) Selected behavioral parameters in mice injected in the dorsal striatum with sgRNA-scr or sgRNA-Chrnb2. n(ctrl)=11-15, n(mutant)=15-19. (D) Y-maze test, alternation score in ctrl vs. mutant mice. 95% CI for the difference between means [-13; 1.4], p=0.11, two-tailed t-test. (E) Novel object recognition test, number of interactions with old and new object in ctrl vs. mutant mice. Effect of genotype: $F_{(1, 58)}$=11, p=0.0013. Number of interactions with old object in ctrl vs. mutant mice, p=0.0496, number of interactions with new object in ctrl vs. mutant mice, p=0.032. Two-way ANOVA with post-hoc Sidak's test. (F) Social interaction test, time interacting with object and mouse stimuli in ctrl vs. mutant mice expressed as percentage of total interaction time. Genotype vs. stimulus interaction: $F_{(1, 62)}$=4.1, p=0.048. Two-way ANOVA. (G) Social preference test, time spent interacting with an object and social stimulus in ctrl vs. mutant mice (left), also expressed as percentage of total interaction time (right). Left graph: Effect of genotype: $F_{(1, 58)}$=4.3, p=0.044. Genotype vs. stimulus interaction: $F_{(1, 58)}$=8.3, p=0.0055. Time spent with object in ctrl vs. mutant mice, p=0.81, time spent with social stimulus in ctrl vs. mutant mice, p=0.0018. Right graph: Genotype vs. stimulus interaction: $F_{(1, 58)}$=24, p<0.0001. Time spent with object in ctrl vs. mutant mice, p=0.0022, time spent with social stimulus in ctrl vs. mutant mice, p=0.0022. Two-way ANOVA followed by post-hoc Sidak's test. (H) Elevated plus maze test, time spent in arms (left) and number of entries into arms (right). Left graph: Genotype vs. arm interaction: $F_{(1, 50)}$=0.075, p=0.79. Right graph: Effect of genotype: $F_{(1, 50)}$=0.14, p=0.71. Two-way ANOVA.

Figure 6

KD of beta2 nicotinic subunit in NPY-Cre-positive striatal neurons leads to changes in explorative, social and anxiety-like behavior. (A) A representative brain section from NPY-Cre::Cas9-GFP mouse showing scattered Cas-GFP expression in the DS. (B) An overview and the order of behavioral tests performed in NPY-Cre::Cas-GFP mice injected with sgRNA-scr (controls) or sgRNA-Chrnb2 (mutants). Tests showing behavioral alterations in mutants are highlighted in blue color. (C-F) Selected behavioral parameters in mice injected in the dorsal striatum with sgRNA-scr or sgRNA-Chrnb2. n(ctrl)=10-11, n(mutant)=10-12. (C) Novel object

recognition test, number of interactions in ctrl vs. mutant mice. Effect of genotype: $F_{(1, 38)}=5.6$, $p=0.022$, two-way ANOVA. (D) Social preference test, percentage of time spent interacting with an object and social stimulus in ctrl vs. mutant mice. Genotype vs. stimulus interaction: $F_{(1, 40)}=5$, $p=0.0303$. Two-way ANOVA. (E) Left: Elevated plus maze, time spent in closed and open/middle arms in ctrl vs. mutant mice. Genotype vs. arm interaction: $F_{(1, 40)}=8.5$, $p=0.0056$, two-way ANOVA. Right: Elevated plus maze, number of entries in closed and open arms in ctrl vs. mutant mice. Effect of genotype: $F_{(1, 40)}=11$, $p=0.0022$. Number of entries in the closed arms in ctrl vs. mutant mice, $p=0.047$, number of entries in the open arms in ctrl vs. mutant mice, $p=0.057$. Two-way ANOVA followed by Sidak's post-hoc test.

References

(1) Albuquerque, E. X.; Pereira, E. F. R.; Alkondon, M.; Rogers, S. W. Mammalian Nicotinic Acetylcholine Receptors: From Structure to Function. *Physiol. Rev.* **2009**, *89* (1), 73–120. https://doi.org/10.1152/physrev.00015.2008.

(2) Wittenberg, R. E.; Wolfman, S. L.; De Biasi, M.; Dani, J. A. Nicotinic Acetylcholine Receptors and Nicotine Addiction: A Brief Introduction. *Neuropharmacology* **2020**, *177*, 108256. https://doi.org/10.1016/j.neuropharm.2020.108256.

(3) Jensen, A. A.; Frølund, B.; Liljefors, T.; Krogsgaard-Larsen, P. Neuronal Nicotinic Acetylcholine Receptors: Structural Revelations, Target Identifications, and Therapeutic Inspirations. *J. Med. Chem.* **2005**, *48* (15), 4705–4745. https://doi.org/10.1021/jm040219e.

(4) Zoli, M.; Pistillo, F.; Gotti, C. Diversity of Native Nicotinic Receptor Subtypes in Mammalian Brain. *Neuropharmacology* **2015**, *96* (Pt B), 302–311. https://doi.org/10.1016/j.neuropharm.2014.11.003.

(5) Terry, A. V.; Jones, K.; Bertrand, D. Nicotinic Acetylcholine Receptors in Neurological and Psychiatric Diseases. *Pharmacol. Res.* **2023**, *191*, 106764. https://doi.org/10.1016/j.phrs.2023.106764.

(6) Poorthuis, R. B.; Bloem, B.; Schak, B.; Wester, J.; de Kock, C. P. J.; Mansvelder, H. D. Layer-Specific Modulation of the Prefrontal Cortex by Nicotinic Acetylcholine Receptors. *Cereb. Cortex N. Y. N 1991* **2013**, *23* (1), 148–161. https://doi.org/10.1093/cercor/bhr390.

(7) Tasic, B.; Yao, Z.; Graybuck, L. T.; Smith, K. A.; Nguyen, T. N.; Bertagnolli, D.; Goldy, J.; Garren, E.; Economo, M. N.; Viswanathan, S.; Penn, O.; Bakken, T.; Menon, V.; Miller, J.; Fong, O.; Hirokawa, K. E.; Lathia, K.; Rimorin, C.; Tieu, M.; Larsen, R.; Casper, T.; Barkan, E.; Kroll, M.; Parry, S.; Shapovalova, N. V.; Hirschstein, D.; Pendergraft, J.; Sullivan, H. A.; Kim, T. K.; Szafer, A.; Dee, N.; Groblewski, P.; Wickersham, I.; Cetin, A.; Harris, J. A.; Levi, B. P.; Sunkin, S. M.; Madisen, L.; Daigle, T. L.; Looger, L.; Bernard, A.; Phillips, J.; Lein, E.; Hawrylycz, M.; Svoboda, K.; Jones, A. R.; Koch, C.; Zeng, H. Shared and Distinct Transcriptomic Cell Types across Neocortical Areas. *Nature* **2018**, *563* (7729), 72–78. https://doi.org/10.1038/s41586-018-0654-5.

(8) Abbondanza, A.; Urushadze, A.; Alves-Barboza, A. R.; Janickova, H. Expression and Function of Nicotinic Acetylcholine Receptors in Specific Neuronal Populations: Focus on Striatal and Prefrontal Circuits. *Pharmacol. Res.* **2024**, *204*, 107190. https://doi.org/10.1016/j.phrs.2024.107190.

(9) Koukouli, F.; Rooy, M.; Tziotis, D.; Sailor, K. A.; O'Neill, H. C.; Levenga, J.; Witte, M.; Nilges, M.; Changeux, J.-P.; Hoeffer, C. A.; Stitzel, J. A.; Gutkin, B. S.; DiGregorio, D. A.; Maskos, U. Nicotine Reverses Hypofrontality in Animal Models of Addiction and Schizophrenia. *Nat. Med.* **2017**, *23* (3), 347–354. https://doi.org/10.1038/nm.4274.

(10) Luo, Y.-F.; Lu, L.; Song, H.-Y.; Xu, H.; Zheng, Z.-W.; Wu, Z.-Y.; Jiang, C.-C.; Tong, C.; Yuan, H.-Y.; Liu, X.-X.; Chen, X.; Sun, M.; Tang, Y.-M.; Fan, H.-Y.; Han, F.; Lu, Y.-M. Divergent Projections of the Prelimbic Cortex Mediate Autism- and Anxiety-like Behaviors. *Mol. Psychiatry* **2023**, *28* (6), 2343–2354. https://doi.org/10.1038/s41380-023-01954-y.

(11) Nestler, E. J.; Russo, S. J. Neurobiological Basis of Stress Resilience. *Neuron* **2024**, *112* (12), 1911–1929. https://doi.org/10.1016/j.neuron.2024.05.001.

(12) Mangerud, W. L.; Bjerkeset, O.; Holmen, T. L.; Lydersen, S.; Indredavik, M. S. Smoking, Alcohol Consumption, and Drug Use among Adolescents with Psychiatric Disorders Compared with a Population Based Sample. *J. Adolesc.* **2014**, *37* (7), 1189–1199. https://doi.org/10.1016/j.adolescence.2014.08.007.
(13) Hartz, S. M.; Horton, A. C.; Hancock, D. B.; Baker, T. B.; Caporaso, N. E.; Chen, L.-S.; Hokanson, J. E.; Lutz, S. M.; Marazita, M. L.; McNeil, D. W.; Pato, C. N.; Pato, M. T.; Johnson, E. O.; Bierut, L. J. Genetic Correlation between Smoking Behaviors and Schizophrenia. *Schizophr. Res.* **2018**, *194*, 86–90. https://doi.org/10.1016/j.schres.2017.02.022.
(14) Bejerot, S.; Nylander, L. Low Prevalence of Smoking in Patients with Autism Spectrum Disorders. *Psychiatry Res.* **2003**, *119* (1–2), 177–182. https://doi.org/10.1016/s0165-1781(03)00123-9.
(15) Power, S. K.; Venkatesan, S.; Lambe, E. K. Xanomeline Restores Endogenous Nicotinic Acetylcholine Receptor Signaling in Mouse Prefrontal Cortex. *Neuropsychopharmacol. Off. Publ. Am. Coll. Neuropsychopharmacol.* **2023**, *48* (4), 671–682. https://doi.org/10.1038/s41386-023-01531-5.
(16) Mineur, Y. S.; Soares, A. R.; Etherington, I. M.; Abdulla, Z. I.; Picciotto, M. R. Pathophysiology of nAChRs: Limbic Circuits and Related Disorders. *Pharmacol. Res.* **2023**, *191*, 106745. https://doi.org/10.1016/j.phrs.2023.106745.
(17) Avale, M. E.; Chabout, J.; Pons, S.; Serreau, P.; De Chaumont, F.; Olivo-Marin, J.-C.; Bourgeois, J.-P.; Maskos, U.; Changeux, J.-P.; Granon, S. Prefrontal Nicotinic Receptors Control Novel Social Interaction between Mice. *FASEB J. Off. Publ. Fed. Am. Soc. Exp. Biol.* **2011**, *25* (7), 2145–2155. https://doi.org/10.1096/fj.10-178558.
(18) Koukouli, F.; Changeux, J.-P. Do Nicotinic Receptors Modulate High-Order Cognitive Processing? *Trends Neurosci.* **2020**, *43* (8), 550–564. https://doi.org/10.1016/j.tins.2020.06.001.
(19) Proulx, E.; Piva, M.; Tian, M. K.; Bailey, C. D. C.; Lambe, E. K. Nicotinic Acetylcholine Receptors in Attention Circuitry: The Role of Layer VI Neurons of Prefrontal Cortex. *Cell. Mol. Life Sci. CMLS* **2014**, *71* (7), 1225–1244. https://doi.org/10.1007/s00018-013-1481-3.
(20) Galvin, V. C.; Arnsten, A. F. T.; Wang, M. Involvement of Nicotinic Receptors in Working Memory Function. *Curr. Top. Behav. Neurosci.* **2020**, *45*, 89–99. https://doi.org/10.1007/7854_2020_142.
(21) dos Santos Coura, R.; Granon, S. Prefrontal Neuromodulation by Nicotinic Receptors for Cognitive Processes. *Psychopharmacology (Berl.)* **2012**, *221* (1), 1–18. https://doi.org/10.1007/s00213-011-2596-6.
(22) Bloem, B.; Poorthuis, R. B.; Mansvelder, H. D. Cholinergic Modulation of the Medial Prefrontal Cortex: The Role of Nicotinic Receptors in Attention and Regulation of Neuronal Activity. *Front. Neural Circuits* **2014**, *8*, 17. https://doi.org/10.3389/fncir.2014.00017.
(23) Porter, J. T.; Cauli, B.; Tsuzuki, K.; Lambolez, B.; Rossier, J.; Audinat, E. Selective Excitation of Subtypes of Neocortical Interneurons by Nicotinic Receptors. *J. Neurosci. Off. J. Soc. Neurosci.* **1999**, *19* (13), 5228–5235. https://doi.org/10.1523/JNEUROSCI.19-13-05228.1999.
(24) Proulx, E.; Piva, M.; Tian, M. K.; Bailey, C. D. C.; Lambe, E. K. Nicotinic Acetylcholine Receptors in Attention Circuitry: The Role of Layer VI Neurons of Prefrontal Cortex. *Cell. Mol. Life Sci. CMLS* **2014**, *71* (7), 1225–1244. https://doi.org/10.1007/s00018-013-1481-3.

(25) Venkatesan, S.; Chen, T.; Liu, Y.; Turner, E. E.; Tripathy, S. J.; Lambe, E. K. Chrna5 and Lynx Prototoxins Identify Acetylcholine Super-Responder Subplate Neurons. *iScience* **2023**, *26* (2), 105992. https://doi.org/10.1016/j.isci.2023.105992.
(26) Falk, E. N.; Norman, K. J.; Garkun, Y.; Demars, M. P.; Im, S.; Taccheri, G.; Short, J.; Caro, K.; McCraney, S. E.; Cho, C.; Smith, M. R.; Lin, H.-M.; Koike, H.; Bateh, J.; Maccario, P.; Waltrip, L.; Janis, M.; Morishita, H. Nicotinic Regulation of Local and Long-Range Input Balance Drives Top-down Attentional Circuit Maturation. *Sci. Adv.* **2021**, *7* (10), eabe1527. https://doi.org/10.1126/sciadv.abe1527.
(27) Karagiannis, A.; Gallopin, T.; Dávid, C.; Battaglia, D.; Geoffroy, H.; Rossier, J.; Hillman, E. M. C.; Staiger, J. F.; Cauli, B. Classification of NPY-Expressing Neocortical Interneurons. *J. Neurosci. Off. J. Soc. Neurosci.* **2009**, *29* (11), 3642–3659. https://doi.org/10.1523/JNEUROSCI.0058-09.2009.
(28) Lee, S.; Hjerling-Leffler, J.; Zagha, E.; Fishell, G.; Rudy, B. The Largest Group of Superficial Neocortical GABAergic Interneurons Expresses Ionotropic Serotonin Receptors. *J. Neurosci. Off. J. Soc. Neurosci.* **2010**, *30* (50), 16796–16808. https://doi.org/10.1523/JNEUROSCI.1869-10.2010.
(29) Burbridge, T. J.; Xu, H.-P.; Ackman, J. B.; Ge, X.; Zhang, Y.; Ye, M.-J.; Zhou, Z. J.; Xu, J.; Contractor, A.; Crair, M. C. Visual Circuit Development Requires Patterned Activity Mediated by Retinal Acetylcholine Receptors. *Neuron* **2014**, *84* (5), 1049–1064. https://doi.org/10.1016/j.neuron.2014.10.051.
(30) Platt, R. J.; Chen, S.; Zhou, Y.; Yim, M. J.; Swiech, L.; Kempton, H. R.; Dahlman, J. E.; Parnas, O.; Eisenhaure, T. M.; Jovanovic, M.; Graham, D. B.; Jhunjhunwala, S.; Heidenreich, M.; Xavier, R. J.; Langer, R.; Anderson, D. G.; Hacohen, N.; Regev, A.; Feng, G.; Sharp, P. A.; Zhang, F. CRISPR-Cas9 Knockin Mice for Genome Editing and Cancer Modeling. *Cell* **2014**, *159* (2), 440–455. https://doi.org/10.1016/j.cell.2014.09.014.
(31) Milstein, A. D.; Bloss, E. B.; Apostolides, P. F.; Vaidya, S. P.; Dilly, G. A.; Zemelman, B. V.; Magee, J. C. Inhibitory Gating of Input Comparison in the CA1 Microcircuit. *Neuron* **2015**, *87* (6), 1274–1289. https://doi.org/10.1016/j.neuron.2015.08.025.
(32) Gong, S.; Doughty, M.; Harbaugh, C. R.; Cummins, A.; Hatten, M. E.; Heintz, N.; Gerfen, C. R. Targeting Cre Recombinase to Specific Neuron Populations with Bacterial Artificial Chromosome Constructs. *J. Neurosci. Off. J. Soc. Neurosci.* **2007**, *27* (37), 9817–9823. https://doi.org/10.1523/JNEUROSCI.2707-07.2007.
(33) Abbondanza, A.; Ribeiro Bas, I.; Modrak, M.; Capek, M.; Minich, J.; Tyshkevich, A.; Naser, S.; Rangotis, R.; Houdek, P.; Sumova, A.; Dumas, S.; Bernard, V.; Janickova, H. Nicotinic Acetylcholine Receptors Expressed by Striatal Interneurons Inhibit Striatal Activity and Control Striatal-Dependent Behaviors. *J. Neurosci. Off. J. Soc. Neurosci.* **2022**, *42* (13), 2786–2803. https://doi.org/10.1523/JNEUROSCI.1627-21.2022.
(34) Dumas, S.; Wallén-Mackenzie, Å. Developmental Co-Expression of Vglut2 and Nurr1 in a Mes-Di-Encephalic Continuum Preceeds Dopamine and Glutamate Neuron Specification. *Front. Cell Dev. Biol.* **2019**, *7*, 307. https://doi.org/10.3389/fcell.2019.00307.
(35) Bankhead, P.; Loughrey, M. B.; Fernández, J. A.; Dombrowski, Y.; McArt, D. G.; Dunne, P. D.; McQuaid, S.; Gray, R. T.; Murray, L. J.; Coleman, H. G.; James, J. A.; Salto-Tellez, M.; Hamilton, P. W. QuPath: Open Source Software for Digital Pathology Image Analysis. *Sci. Rep.* **2017**, *7* (1), 16878. https://doi.org/10.1038/s41598-017-17204-5.

(36) Franklin, K. B. J.; Paxinos, G. *The Mouse Brain in Stereotaxic Coordinates*; Boston, 2008.
(37) Peng, C.; Yan, Y.; Kim, V. J.; Engle, S. E.; Berry, J. N.; McIntosh, J. M.; Neve, R. L.; Drenan, R. M. Gene Editing Vectors for Studying Nicotinic Acetylcholine Receptors in Cholinergic Transmission. *Eur. J. Neurosci.* **2019**, *50* (3), 2224–2238. https://doi.org/10.1111/ejn.13957.
(38) Swiech, L.; Heidenreich, M.; Banerjee, A.; Habib, N.; Li, Y.; Trombetta, J.; Sur, M.; Zhang, F. In Vivo Interrogation of Gene Function in the Mammalian Brain Using CRISPR-Cas9. *Nat. Biotechnol.* **2015**, *33* (1), 102–106. https://doi.org/10.1038/nbt.3055.
(39) Lowry, O. H.; Rosebrough, N. J.; Farr, A. L.; Randall, R. J. Protein Measurement with the Folin Phenol Reagent. *J. Biol. Chem.* **1951**, *193* (1), 265–275.
(40) Martinez-Marquez, E.; Reyes-Leon, S.; Garcia-San-Jose, F.; Lopez-Begines, S.; Nieto-Gonzalez, J. L.; Garcia-Junco-Clemente, P. Cholinergic Modulation of Chandelier Cells via Heteromeric Nicotinic Receptors in Prefrontal Cortex. bioRxiv January 18, 2025, p 2025.01.18.633708. https://doi.org/10.1101/2025.01.18.633708.
(41) Dellal, S.; Zurita, H.; Kruglikov, I.; Valero, M.; Abad-Perez, P.; Geron, E.; Meng, J. H.; Prönneke, A.; Hanson, J. L.; Mir, E.; Ongaro, M.; Wang, X.-J.; Buzsáki, G.; Machold, R.; Rudy, B. Inhibitory and Disinhibitory VIP IN-Mediated Circuits in Neocortex. bioRxiv May 17, 2025, p 2025.02.26.640383. https://doi.org/10.1101/2025.02.26.640383.
(42) Saffari, R.; Teng, Z.; Zhang, M.; Kravchenko, M.; Hohoff, C.; Ambrée, O.; Zhang, W. NPY+-, but Not PV+- GABAergic Neurons Mediated Long-Range Inhibition from Infra- to Prelimbic Cortex. *Transl. Psychiatry* **2016**, *6* (2), e736. https://doi.org/10.1038/tp.2016.7.
(43) Xie, Z.; Li, D.; Cheng, X.; Pei, Q.; Gu, H.; Tao, T.; Huang, M.; Shang, C.; Geng, D.; Zhao, M.; Liu, A.; Zhang, C.; Zhang, F.; Ma, Y.; Cao, P. A Brain-to-Spinal Sensorimotor Loop for Repetitive Self-Grooming. *Neuron* **2022**, *110* (5), 874-890.e7. https://doi.org/10.1016/j.neuron.2021.11.028.
(44) Spanò, T.; Nassim-Assir, B.; Kaulich, E.; Tushev, G.; Fürst, N.; Will, H.; Marić, L.; Ciirdaeva, E.; Schuman, E. M. Localized mRNAs and Protein Synthesis in Cortical Layer 1. bioRxiv November 24, 2025, p 2025.11.23.689989. https://doi.org/10.1101/2025.11.23.689989.
(45) Letzkus, J. J.; Wolff, S. B. E.; Meyer, E. M. M.; Tovote, P.; Courtin, J.; Herry, C.; Lüthi, A. A Disinhibitory Microcircuit for Associative Fear Learning in the Auditory Cortex. *Nature* **2011**, *480* (7377), 331–335. https://doi.org/10.1038/nature10674.
(46) Lara, A. H.; Wallis, J. D. The Role of Prefrontal Cortex in Working Memory: A Mini Review. *Front. Syst. Neurosci.* **2015**, *9*, 173. https://doi.org/10.3389/fnsys.2015.00173.
(47) Guillem, K.; Bloem, B.; Poorthuis, R. B.; Loos, M.; Smit, A. B.; Maskos, U.; Spijker, S.; Mansvelder, H. D. Nicotinic Acetylcholine Receptor B2 Subunits in the Medial Prefrontal Cortex Control Attention. *Science* **2011**, *333* (6044), 888–891. https://doi.org/10.1126/science.1207079.
(48) Spanò, T.; Nassim-Assir, B.; Kaulich, E.; Tushev, G.; Fürst, N.; Will, H.; Marić, L.; Ciirdaeva, E.; Schuman, E. M. Localized mRNAs and Protein Synthesis in Cortical Layer 1. bioRxiv November 24, 2025, p 2025.11.23.689989. https://doi.org/10.1101/2025.11.23.689989.
(49) Bicks, L. K.; Yamamuro, K.; Flanigan, M. E.; Kim, J. M.; Kato, D.; Lucas, E. K.; Koike, H.; Peng, M. S.; Brady, D. M.; Chandrasekaran, S.; Norman, K. J.; Smith, M. R.; Clem, R. L.; Russo, S. J.; Akbarian, S.; Morishita, H. Prefrontal Parvalbumin Interneurons Require Juvenile Social

Experience to Establish Adult Social Behavior. *Nat. Commun.* **2020**, *11* (1), 1003. https://doi.org/10.1038/s41467-020-14740-z.
(50) Jeon, Y.-S.; Jeong, D.; Kweon, H.; Kim, J.-H.; Kim, C. Y.; Oh, Y.; Lee, Y.-H.; Kim, C. H.; Kim, S.-G.; Jeong, J.-W.; Kim, E.; Lee, S.-H. Adolescent Parvalbumin Expression in the Left Orbitofrontal Cortex Shapes Sociability in Female Mice. *J. Neurosci. Off. J. Soc. Neurosci.* **2023**, *43* (9), 1555–1571. https://doi.org/10.1523/JNEUROSCI.0918-22.2023.
(51) Qi, C.; Sima, W.; Mao, H.; Hu, E.; Ge, J.; Deng, M.; Chen, A.; Ye, W.; Xue, Q.; Wang, W.; Chen, Q.; Wu, S. Anterior Cingulate Cortex Parvalbumin and Somatostatin Interneurons Shape Social Behavior in Male Mice. *Nat. Commun.* **2025**, *16* (1), 4156. https://doi.org/10.1038/s41467-025-59473-z.
(52) Phenis, D.; Vunck, S. A.; Valentini, V.; Arias, H.; Schwarcz, R.; Bruno, J. P. Activation of Alpha7 Nicotinic and NMDA Receptors Is Necessary for Performance in a Working Memory Task. *Psychopharmacology (Berl.)* **2020**, *237* (6), 1723–1735. https://doi.org/10.1007/s00213-020-05495-y.
(53) Valentine, G.; Sofuoglu, M. Cognitive Effects of Nicotine: Recent Progress. *Curr. Neuropharmacol.* **2018**, *16* (4), 403–414. https://doi.org/10.2174/1570159X15666171103152136.
(54) Maskos, U.; Molles, B. E.; Pons, S.; Besson, M.; Guiard, B. P.; Guilloux, J.-P.; Evrard, A.; Cazala, P.; Cormier, A.; Mameli-Engvall, M.; Dufour, N.; Cloëz-Tayarani, I.; Bemelmans, A.-P.; Mallet, J.; Gardier, A. M.; David, V.; Faure, P.; Granon, S.; Changeux, J.-P. Nicotine Reinforcement and Cognition Restored by Targeted Expression of Nicotinic Receptors. *Nature* **2005**, *436* (7047), 103–107. https://doi.org/10.1038/nature03694.
(55) Maubourguet, N.; Lesne, A.; Changeux, J.-P.; Maskos, U.; Faure, P. Behavioral Sequence Analysis Reveals a Novel Role for Beta2* Nicotinic Receptors in Exploration. *PLoS Comput. Biol.* **2008**, *4* (11), e1000229. https://doi.org/10.1371/journal.pcbi.1000229.
(56) Nguyen, C.; Mondoloni, S.; Le Borgne, T.; Centeno, I.; Come, M.; Jehl, J.; Solié, C.; Reynolds, L. M.; Durand-de Cuttoli, R.; Tolu, S.; Valverde, S.; Didienne, S.; Hannesse, B.; Fiancette, J.-F.; Pons, S.; Maskos, U.; Deroche-Gamonet, V.; Dalkara, D.; Hardelin, J.-P.; Mourot, A.; Marti, F.; Faure, P. Nicotine Inhibits the VTA-to-Amygdala Dopamine Pathway to Promote Anxiety. *Neuron* **2021**, *109* (16), 2604-2615.e9. https://doi.org/10.1016/j.neuron.2021.06.013.
(57) Picciotto, M. R.; Lewis, A. S.; van Schalkwyk, G. I.; Mineur, Y. S. Mood and Anxiety Regulation by Nicotinic Acetylcholine Receptors: A Potential Pathway to Modulate Aggression and Related Behavioral States. *Neuropharmacology* **2015**, *96* (Pt B), 235–243. https://doi.org/10.1016/j.neuropharm.2014.12.028.
(58) Mineur, Y. S.; Mose, T. N.; Maibom, K. L.; Pittenger, S. T.; Soares, A. R.; Wu, H.; Taylor, S. R.; Huang, Y.; Picciotto, M. R. ACh Signaling Modulates Activity of the GABAergic Signaling Network in the Basolateral Amygdala and Behavior in Stress-Relevant Paradigms. *Mol. Psychiatry* **2022**, *27* (12), 4918–4927. https://doi.org/10.1038/s41380-022-01749-7.
(59) Chebolu, S.; Dayan, P.; Lloyd, K. Vigilance, Arousal, and Acetylcholine: Optimal Control of Attention in a Simple Detection Task. *PLoS Comput. Biol.* **2022**, *18* (10), e1010642. https://doi.org/10.1371/journal.pcbi.1010642.
(60) Reichmann, F.; Holzer, P. Neuropeptide Y: A Stressful Review. *Neuropeptides* **2016**, *55*, 99–109. https://doi.org/10.1016/j.npep.2015.09.008.

(61) Casello, S. M.; Flores, R. J.; Yarur, H. E.; Wang, H.; Awanyai, M.; Arenivar, M. A.; Jaime-Lara, R. B.; Bravo-Rivera, H.; Tejeda, H. A. Neuropeptide System Regulation of Prefrontal Cortex Circuitry: Implications for Neuropsychiatric Disorders. *Front. Neural Circuits* **2022**, *16*, 796443. https://doi.org/10.3389/fncir.2022.796443.
(62) Gruber, T. D.; Krishnamurthy, C.; Grimm, J. B.; Tadross, M. R.; Wysocki, L. M.; Gartner, Z. J.; Lavis, L. D. Cell-Specific Chemical Delivery Using a Selective Nitroreductase-Nitroaryl Pair. *ACS Chem. Biol.* **2018**, *13* (10), 2888–2896. https://doi.org/10.1021/acschembio.8b00524.
(63) Shields, B. C.; Yan, H.; Lim, S. S. X.; Burwell, S. C. V.; Cammarata, C. M.; Fleming, E. A.; Yousefzadeh, S. A.; Goldenshtein, V. Z.; Kahuno, E. W.; Vagadia, P. P.; Loughran, M. H.; Zhiquan, L.; McDonnell, M. E.; Scalabrino, M. L.; Thapa, M.; Hawley, T. M.; Field, G. D.; Hull, C.; Schiltz, G. E.; Glickfeld, L. L.; Reitz, A. B.; Tadross, M. R. DART.2: Bidirectional Synaptic Pharmacology with Thousandfold Cellular Specificity. *Nat. Methods* **2024**, *21* (7), 1288–1297. https://doi.org/10.1038/s41592-024-02292-9.
(64) Shields, B. C.; Kahuno, E.; Kim, C.; Apostolides, P. F.; Brown, J.; Lindo, S.; Mensh, B. D.; Dudman, J. T.; Lavis, L. D.; Tadross, M. R. Deconstructing Behavioral Neuropharmacology with Cellular Specificity. *Science* **2017**, *356* (6333), eaaj2161. https://doi.org/10.1126/science.aaj2161.

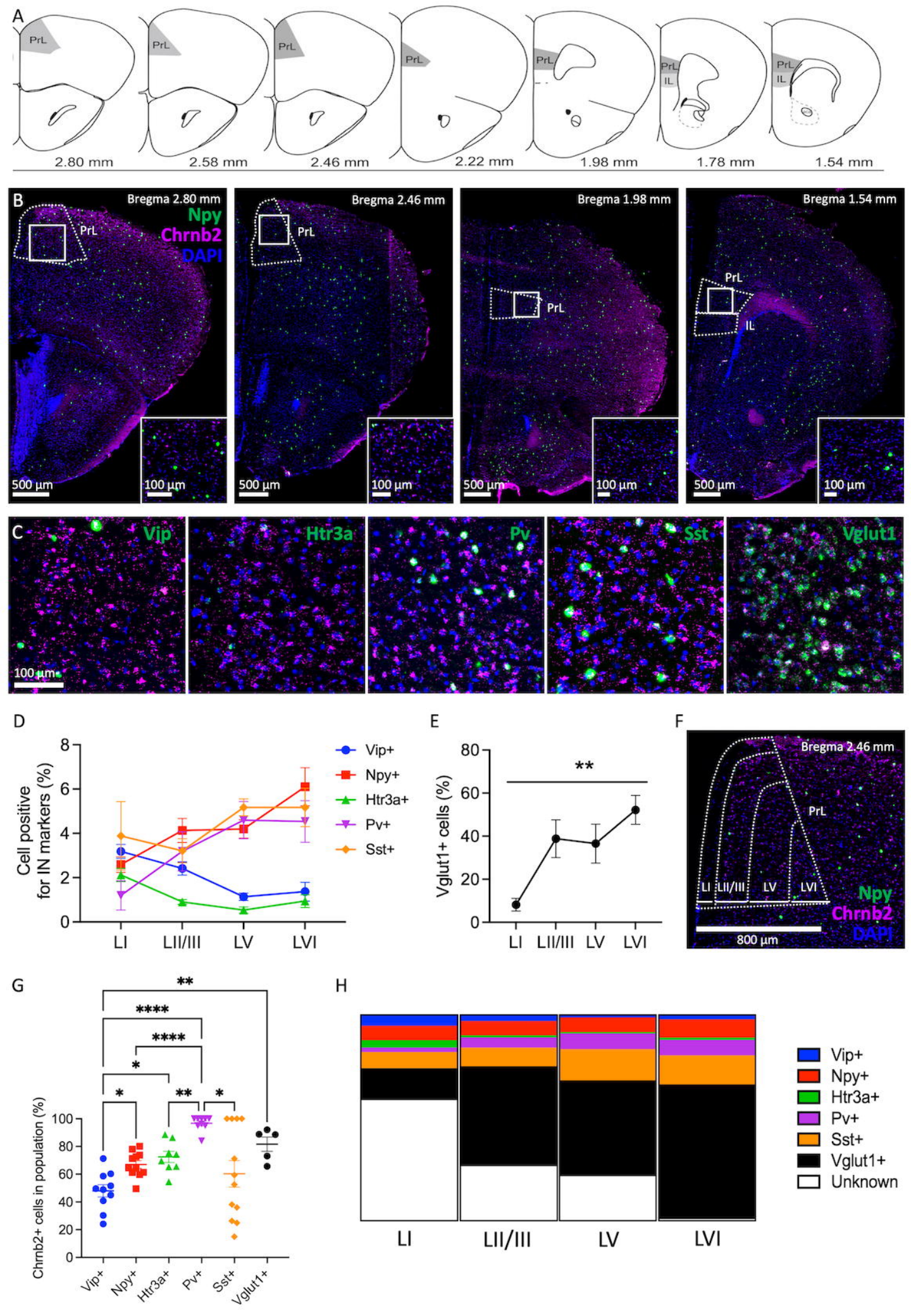
A
PrL
IL
2.80 mm
2.58 mm
2.46 mm
2.22 mm
1.98 mm
1.78 mm
1.54 mm
B
Bregma 2.80 mm
Bregma 2.46 mm
Bregma 1.98 mm
Bregma 1.54 mm
Npy
Chrnb2
DAPI
500 µm
100 µm
C
Vip
Htr3a
Pv
Sst
Vglut1
D
Cell positive for IN markers (%)
Vip+
Npy+
Htr3a+
Pv+
Sst+
LI
LII/III
LV
LVI
E
Vglut1+ cells (%)
**
F
800 µm
G
Chrnb2+ cells in population (%)
Vip+
Npy+
Htr3a+
Pv+
Sst+
Vglut1+
H
Vglut1+
Unknown

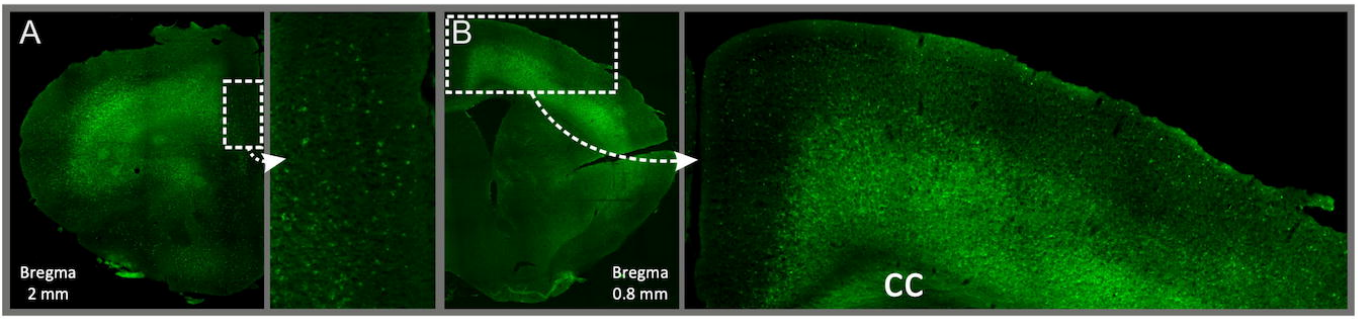
A
Bregma
2 mm
B
Bregma
0.8 mm
CC

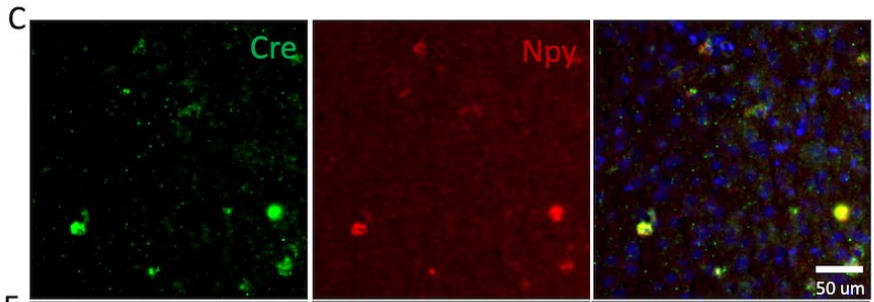
C
Cre
Npy
50 um

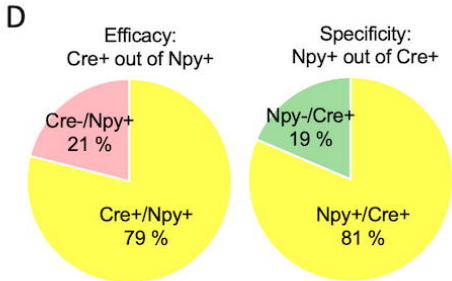
D
Efficacy:
Cre+ out of Npy+
Cre-/Npy+
21 %
Cre+/Npy+
79 %
Specificity:
Npy+ out of Cre+
Npy-/Cre+
19 %
Npy+/Cre+
81 %

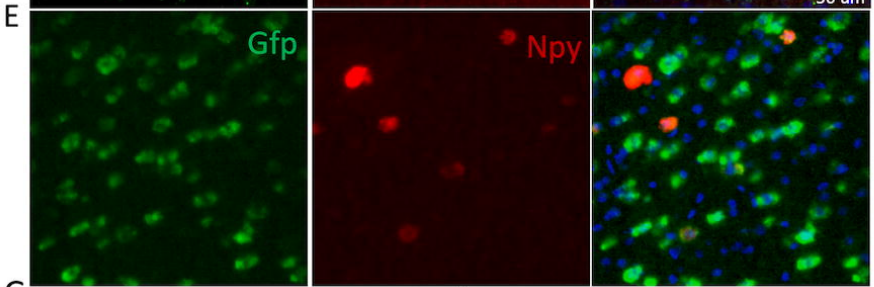
E
Gfp
Npy

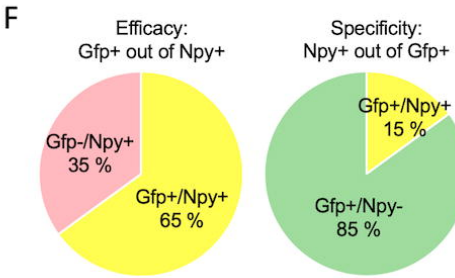
F
Efficacy:
Gfp+ out of Npy+
Gfp-/Npy+
35 %
Gfp+/Npy+
65 %
Specificity:
Npy+ out of Gfp+
Gfp+/Npy+
15 %
Gfp+/Npy-
85 %

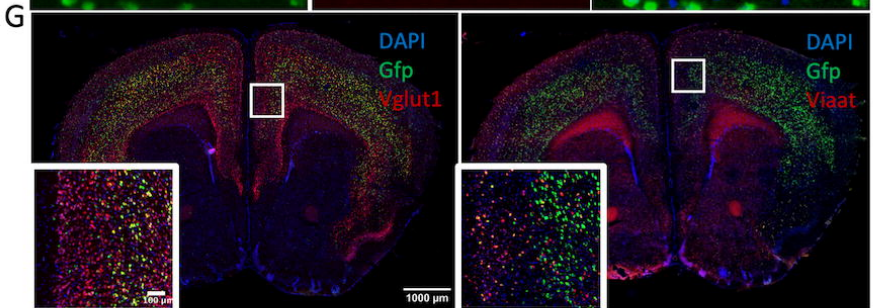
G
DAPI
Gfp
Vglut1
100 µm
1000 µm
DAPI
Gfp
Viaat

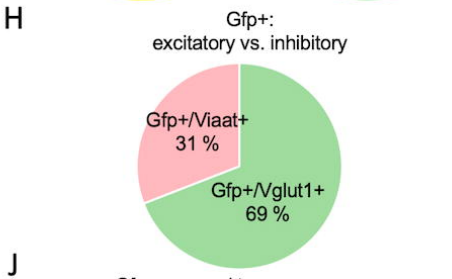
H
Gfp+:
excitatory vs. inhibitory
Gfp+/Viaat+
31 %
Gfp+/Vglut1+
69 %

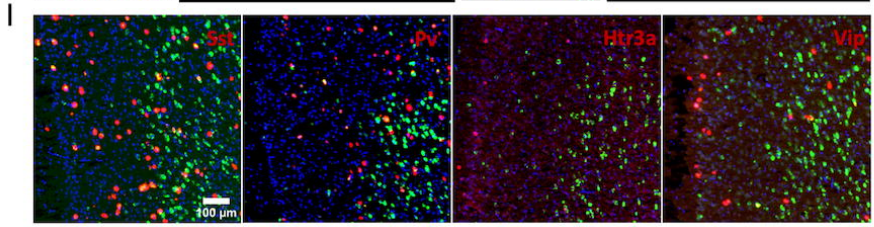
I
Sst
Pv
Htr3a
Vip
100 µm

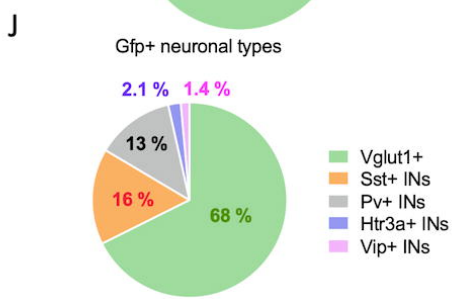
J
Gfp+ neuronal types
2.1 %
1.4 %
13 %
16 %
68 %
Vglut1+
Sst+ INs
Pv+ INs
Htr3a+ INs
Vip+ INs

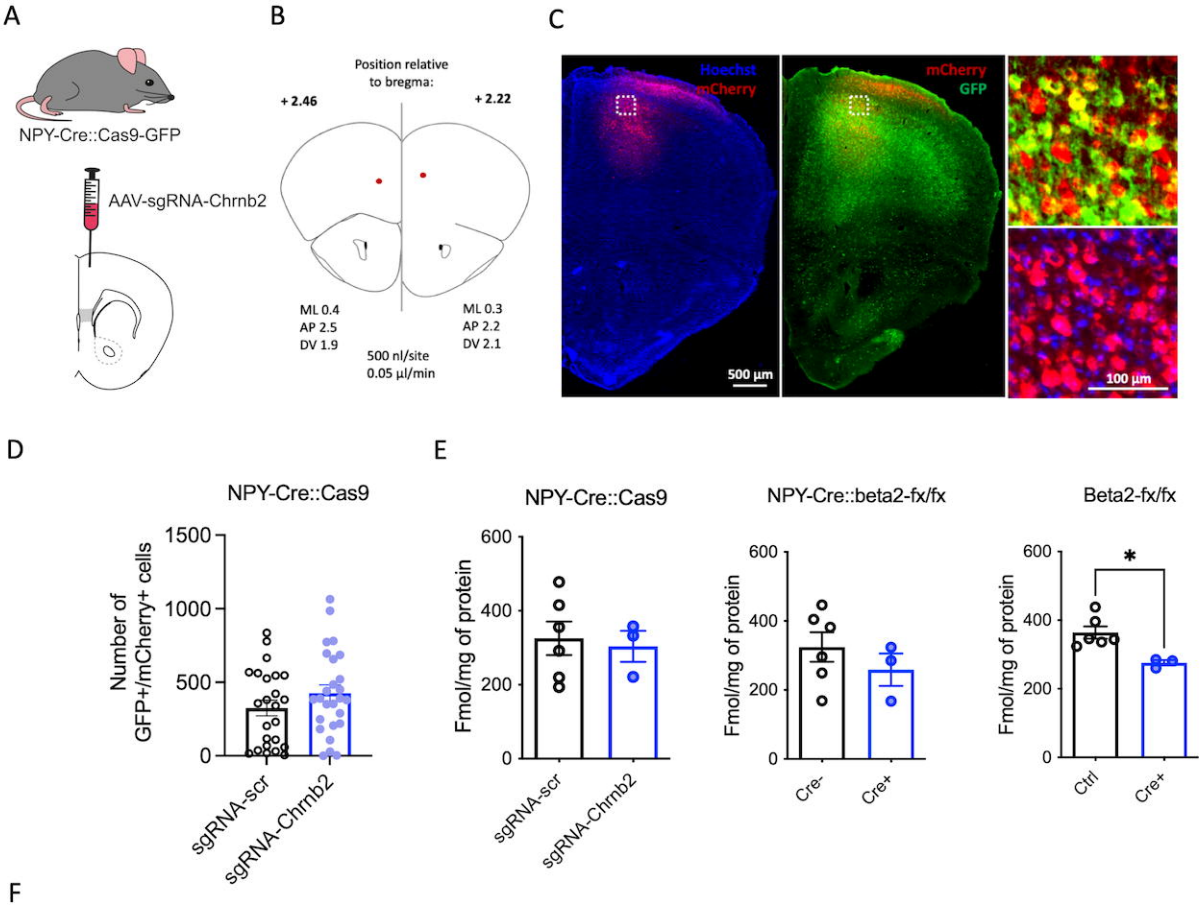
A
NPY-Cre::Cas9-GFP
AAV-sgRNA-Chrnb2
B
Position relative to bregma:
+ 2.46
+ 2.22
ML 0.4
AP 2.5
DV 1.9
ML 0.3
AP 2.2
DV 2.1
500 nl/site
0.05 µl/min
C
Hoechst
mCherry
mCherry
GFP
500 µm
100 µm
D
NPY-Cre::Cas9
Number of GFP+/mCherry+ cells
1500
1000
500
0
sgRNA-scr
sgRNA-Chrnb2
E
NPY-Cre::Cas9
NPY-Cre::beta2-fx/fx
Beta2-fx/fx
Fmol/mg of protein
600
400
200
0
sgRNA-scr
sgRNA-Chrnb2
Cre-
Cre+
Ctrl
Cre+
*
F
PFC sgRNA-Chrnb2
PFC sgRNA-scr
PFC NO injection
PFC sgRNA-Chrnb2
PFC sgRNA-scr
Striatum sgRNA-Chrnb2

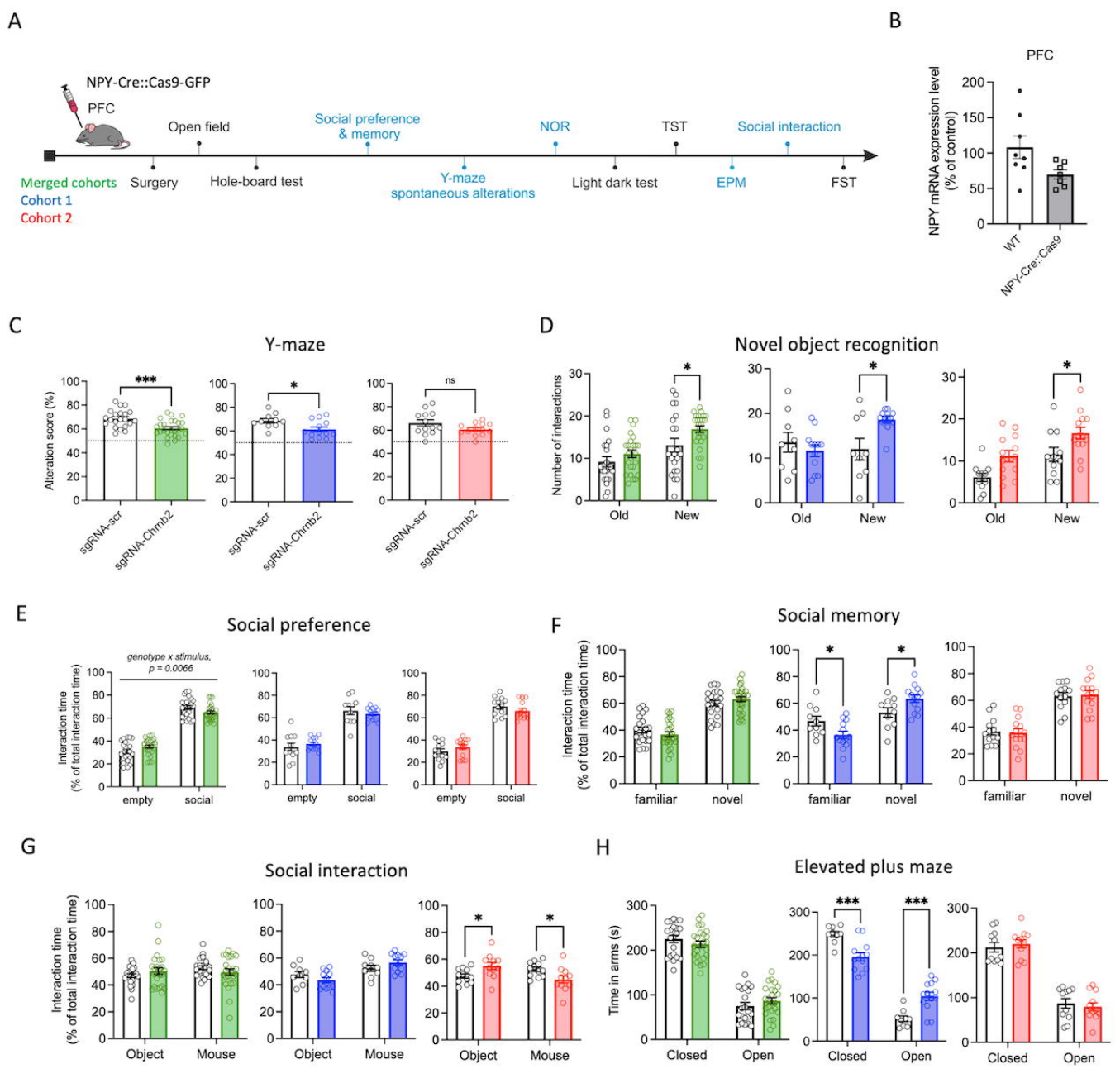
A
NPY-Cre::Cas9-GFP
PFC
Open field
Social preference & memory
NOR
TST
Social interaction
Merged cohorts
Cohort 1
Cohort 2
Surgery
Hole-board test
Y-maze spontaneous alterations
Light dark test
EPM
FST
B
PFC
NPY mRNA expression level (% of control)
WT
NPY-Cre::Cas9
C
Y-maze
Alteration score (%)
sgRNA-scr
sgRNA-Chrnb2
D
Novel object recognition
Number of interactions
Old
New
E
Social preference
genotype x stimulus, p = 0.0066
Interaction time (% of total interaction time)
empty
social
F
Social memory
familiar
novel
G
Social interaction
Object
Mouse
H
Elevated plus maze
Time in arms (s)
Closed
Open

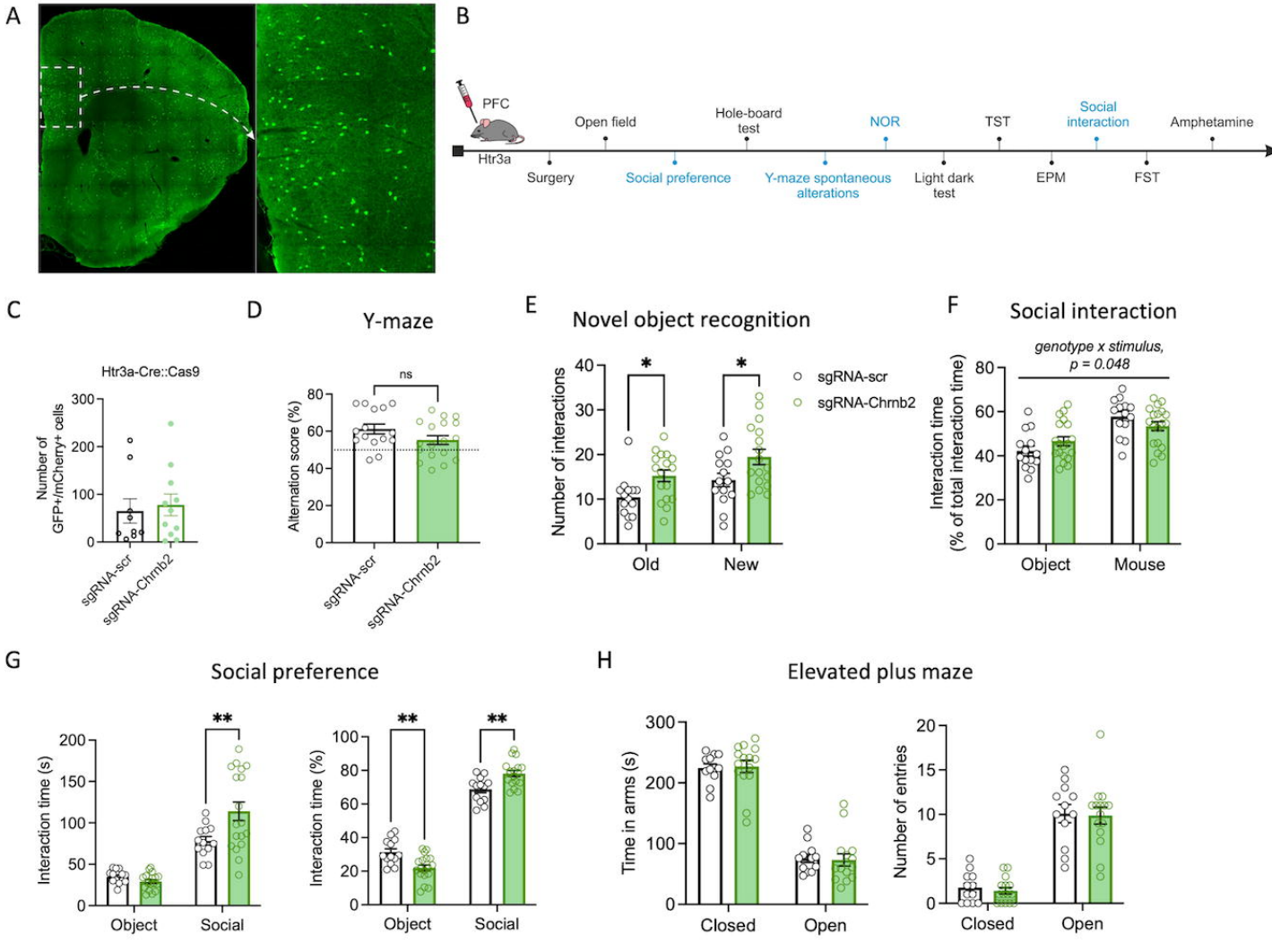
A
B
PFC
Htr3a
Surgery
Open field
Social preference
Hole-board test
Y-maze spontaneous alterations
NOR
Light dark test
TST
EPM
Social interaction
FST
Amphetamine
C
Htr3a-Cre::Cas9
Number of GFP+/mCherry+ cells
sgRNA-scr
sgRNA-Chrnb2
D
Y-maze
ns
Alternation score (%)
sgRNA-scr
sgRNA-Chrnb2
E
Novel object recognition
Number of interactions
sgRNA-scr
sgRNA-Chrnb2
Old
New
F
Social interaction
genotype x stimulus, p = 0.048
Interaction time (% of total interaction time)
Object
Mouse
G
Social preference
Interaction time (s)
Interaction time (%)
Object
Social
H
Elevated plus maze
Time in arms (s)
Number of entries
Closed
Open

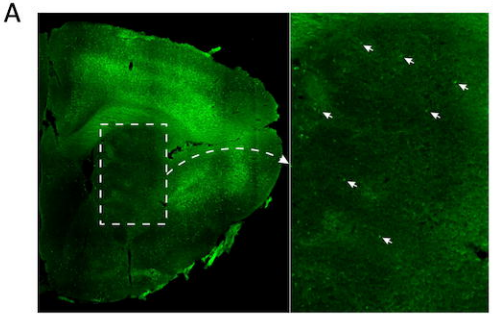
A

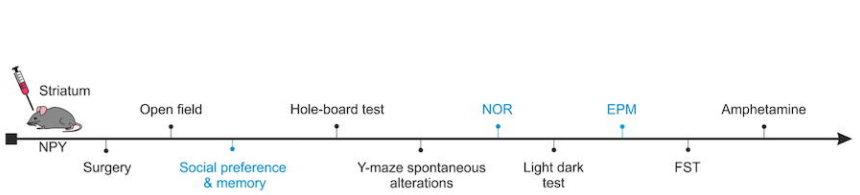
B
Striatum
NPY
Surgery
Open field
Social preference & memory
Hole-board test
Y-maze spontaneous alterations
NOR
Light dark test
EPM
FST
Amphetamine

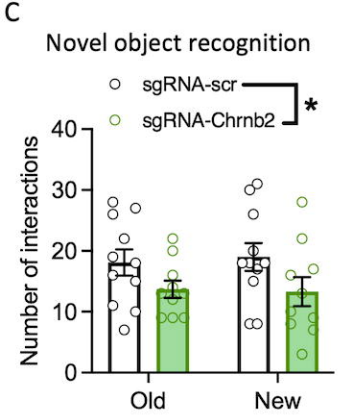
C
Novel object recognition
sgRNA-scr
sgRNA-Chrnb2
*
Number of interactions
40
30
20
10
0
Old
New

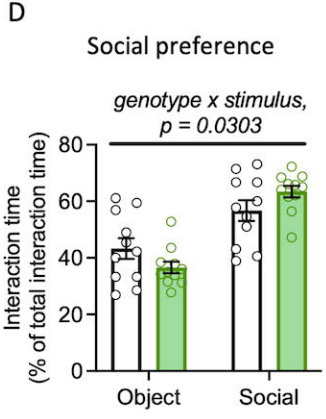
D
Social preference
genotype x stimulus,
p = 0.0303
Interaction time
(% of total interaction time)
80
60
40
20
0
Object
Social

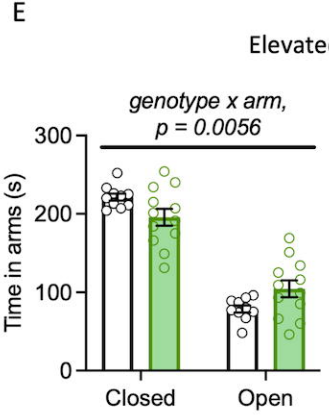
E
Elevated plus maze
genotype x arm,
p = 0.0056
Time in arms (s)
300
200
100
0
Closed
Open

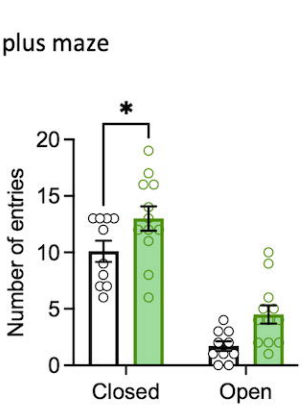
*
Number of entries
20
15
10
5
0
Closed
Open